Efficient Segmentation of Lung Abnormalities in CT Images

Aryaz Baradarani and Q.M. Jonathan Wu

University of Windsor, Ontario, N9B3P4
aryaz@ieee.org, jwu@uwindsor.ca
http://web2.uwindsor.ca/engineering/cvss

Abstract. This paper introduces an efficient technique for lung abnormalities segmentation in CT images based on the use of dual-tree complex wavelet transform (DT-CWT) and multilevel histogram thresholding. Recently, a scalar wavelet-based method has shown favorable results compared with previous approaches in honeycomb detection in pediatric CT images. Using our recently designed dual-tree complex filter bank and employing high resolution intensity similarities, we show that DT-CWT outperforms the results obtained with discrete wavelet transform (DWT) in general. Our early experiments show that multi-wavelets (MW) can also present a promising performance than DWT. The results indicate that DT-CWT performs slightly better than multi-wavelets, however, it can significantly outperform scalar wavelets. The former is probably due to better edge preserving property of multi-wavelets, while the latter is obtained because of good directionality and shift-invariance of dual-tree complex wavelet transform.

Keywords: Segmentation, dual-tree complex wavelets, CT images, lung abnormality, multilevel thresholding.

1 Introduction

Detection, segmentation and analysis of CT (Computerized Tomography) images are important tasks in diagnosing several diseases. Variety and number of images and subimages, even in a particular case, require the necessity of efficient automatic techniques to correctly detect and segment abnormalities so that further high level processing can be performed. Using dual-tree complex wavelet transform (DT-CWT), it is possible to significantly reduce the number of incorrectly detected points, and to improve segmentation stage because of the shift-invariance and good directionality of DT-CWT [12]. Several authors have demonstrated different methods on segmentation of CT images. An adaptive multiple feature method has been suggested in [16] using statistical parameters for classification. The method fails to show a good performance for honeycomb region detection and it is case sensitive with respect to the type of abnormality. We refer to a tutorial by Sluimer et al. [14] on computer analysis of CT images of lung. Recently, Shojaii et al. [13] have shown a wavelet-based

M. Kamel and A. Campilho (Eds.): ICIAR 2009, LNCS 5627, pp. 749–758, 2009.

approach for lung segmentation in pediatric CT images. They used vertical subbands data obtained using the discrete wavelet transform (DWT) to detect honeycomb regions in the wavelet domain, while they found the remaining subbands redundant.

Generally, wavelet bases are optimal for the category of one dimensional signals. In case of 2D (two dimensional), however, DWT cannot be an optimal choice [12] because of the weak line (curve)-singularities of separable wavelets (DWT) in contrast with the efficient point-singularities of wavelets, although DWT is still better than the discrete cosine transform (DCT) while the DWT excels in JPEG2000 compression standard. The recent developments in wavelet-based research have addressed the theory, design and implementation of 2D multi-resolution transforms that can present processing goals more efficiently than those obtained using separable wavelet transform. Curvelets, multi-wavelets, directional filter banks, complex filter banks, steerable pyramid, and finally dual-tree complex wavelet transform are new aspects after the separable wavelet transform. Depending on application, these transforms can offer superior results for image processing purposes rather than discrete wavelet transform.

We proposed the use of multi-wavelets [2] for moving object detection and segmentation, where multi-wavelets outperform the methods in [7] [8]. The problem of object segmentation resembles that of a denoising problem where both multi-wavelets and DT-CWT offer good solutions to denoising problems [12] [15]. The dual-tree wavelet transform is nearly shift-invariant and isolates edges with different directions in different subbands. Motivated by these facts, we develop an automatic DT-CWT based method for detection and segmentation of abnormalities in CT images employing our recently designed 9/7–10/8 dual-tree complex filter bank [17]. The method is based on determining the detection mask in the complex wavelet domain using multilevel histogram thresholding and intensity similarities [6].

2 The 9/7-10/8 Dual-Tree Complex Filter Bank

In this Section we introduce our recently designed dual-tree complex filter bank. Consider the two-channel dual-tree filter bank implementation of the complex wavelet transform. Shown in Fig. 1(a), the primal filter bank $\mathbf{B}$ in each level defines the real part of the wavelet transform. The dual filter bank $\widetilde{\mathbf{B}}$ shown in Fig. 1(b) defines the imaginary part. Recall that the scaling and wavelet functions associated with the analysis side of $\mathbf{B}$ are defined by the two-scale equations $\phi_h(t) = 2\sum_n h_0[n]\phi_h(2t-n)$ and $\psi_h(t) = 2\sum_n h_1[n]\phi_h(2t-n)$, respectively. The scaling function ϕ_f and wavelet function ψ_f in the synthesis side of $\mathbf{B}$ are similarly defined via f_0 and f_1. The same is true for the scaling functions ($\widetilde{\phi}_h$ and $\widetilde{\phi}_f$) and wavelet functions ($\widetilde{\psi}_h$ and $\widetilde{\psi}_f$) of the dual filter bank $\widetilde{\mathbf{B}}$. The dual-tree filter bank defines analytic complex wavelets $\psi_h + j\widetilde{\psi}_h$ and $\widetilde{\psi}_f + j\psi_f$, if the wavelet

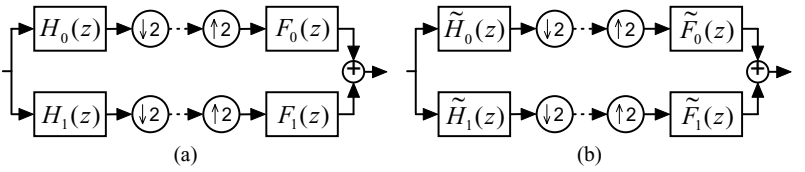

Fig. 1. (a) The primal filter bank $\mathbf{B}$; (b) The dual filter bank $\widetilde{\mathbf{B}}$

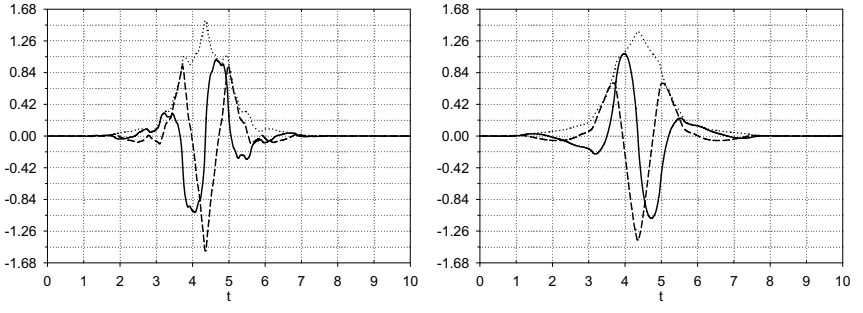

Fig. 2. Wavelets of the dual-tree complex filter bank 9/7–10/8. (a) Analysis side: $\psi_h(t)$ (dashed line), $\widetilde{\psi}_h(t)$ (solid line), and $|\psi_h(t) + j\widetilde{\psi}_h(t)|$ (dotted line); (b) Synthesis side: $\psi_f(t)$ (dashed line), $\widetilde{\psi}_f(t)$ (solid line), and $|\psi_f(t) + j\widetilde{\psi}_f(t)|$ (dotted line).

functions of the two filter banks form Hilbert transform pairs. Specifically, the analysis wavelet $\widetilde{\psi}_h(t)$ of $\widetilde{\mathbf{B}}$ is the Hilbert transform of the analysis wavelet $\psi_h(t)$ of $\mathbf{B}$, and the synthesis wavelet $\psi_f(t)$ of $\mathbf{B}$ is the Hilbert transform of $\widetilde{\psi}_f(t)$. That is, $\widetilde{\Psi}_h(\omega) = -j\mathtt{sign}(\omega)\Psi_h(\omega)$ and $\Psi_f(\omega) = -j\mathtt{sign}(\omega)\widetilde{\Psi}_f(\omega)$, where $\Psi_h(\omega)$, $\Psi_f(\omega)$, $\widetilde{\Psi}_h(\omega)$, and $\widetilde{\Psi}_f(\omega)$ are the Fourier transforms of wavelet functions $\psi_h(t)$, $\psi_f(t)$, $\widetilde{\psi}_h(t)$, and $\widetilde{\psi}_f(t)$ respectively, and $\mathtt{sign}$ represents the signum function. This introduces limited redundancy and allows the transform to provide approximate shift-invariance and more directionality selection of filters [9] [12] while preserving the usual properties of perfect reconstruction and computational efficiency with good frequency responses. It should be noted that these properties are missing in the discrete wavelet transform.

The analysis and synthesis scaling filters of the primal (9/7) and dual (10/8) filter banks are denoted by h_0, f_0, $\widetilde{h}_0$ and $\widetilde{f}_0$, respectively (Table 1). Both the primal and dual filter banks are biorthogonal and exactly symmetric. The analysis wavelets $\psi_h(t)$ and $\widetilde{\psi}_h(t)$ are shown in Fig. 2(a) which also shows the magnitude of the complex function $\psi_h(t)+j\widetilde{\psi}_h(t)$. Fig. 2(b) gives the wavelets $\psi_f(t)$, $\widetilde{\psi}_f(t)$, and $|\psi_f(t)+j\widetilde{\psi}_f(t)|$ in the synthesis side. It should be noted that the magnitude spectra plot of the complex wavelets $\psi_h(t)+j\widetilde{\psi}_h(t)$ and $\psi_f(t)+j\widetilde{\psi}_f(t)$ are essentially one-sided [12] [17]. This implies that the wavelet bases form (approximate) Hilbert transform pairs.

Table 1. The scaling filters of the primal and dual filter banks of 9/7–10/8

n	$h_0[n]$	$f_0[n]$	$\widetilde{h}_0[n]$	$\widetilde{f}_0[n]$
0	-0.06453888262894	0.03782845550700	-0.01600304316399	0.01122570165035
1	-0.04068941760956	-0.02384946501938	-0.06216012765312	0.02159461406422
2	0.41809227322221	-0.11062440441842	0.09484595867485	-0.07043050375330
3	0.78848561640566	0.37740285561265	0.48331721214226	0.03383167141896
4	0.41809227322221	0.85269867900940	0.48331721214226	0.50377851661977
5	-0.04068941760956	0.37740285561265	0.09484595867485	0.50377851661977
6	-0.06453888262894	-0.11062440441842	-0.06216012765312	0.03383167141896
7		-0.02384946501938	-0.01600304316399	-0.07043050375330
8		0.03782845550700		0.02159461406422
9				0.01122570165035

3 Segmentation of Lung Abnormalities

3.1 Design Algorithm

Motivated by our early MW-based approach [2] and the success of 9/7–10/8 in moving object detection and segmentation [1], we develop an efficient algorithm using dual-tree complex wavelet transform and the 9/7–10/8 filter bank employing histogram thresholding in complex wavelet domain to extract abnormalities such as honeycombs and tumors in high resolution CT images. Using the well-known watershed transform [6], lung regions are extracted from the chest image. Fig. 4(a) shows a CT image of chest for a healthy lung, and Figs. 4(b), 4(c), and 4(d) are abnormal lungs with honeycombs, tumorous, and cavity plus cancer, respectively. Mask of lung which is obtained by original image segmentation is used to determine the histogram of subbands in order to calculate the required threholds in each subband. The value of threshold is generally selected in accordance to the location of abnormalities intensity in the respective histogram of a CT image. For instance, honeycombs are a kind of cysts filled with air and therefore they are seen as dark holes. Thus, the value of threshold can be selected as the location of minima in histogram. The details of histogram thresholding can be found in [6]. It should be noted that vessel branches are also high resolution areas and will be extracted along with thresholding step. The vessels removal part of the problem can be cast as a denoising problem. The aim here is to detect as many abnormalities as possible and at the same time suppress the vessel branches areas.

Block diagram of the proposed algorithm is depicted in Fig. 3. CT images in spatial domain are transformed to complex wavelet domain in the respective subbands up to the last subband depending on the number of levels the decomposition stage may be grown up. We use a two level dual-tree structure with the 9/7–10/8 filter bank embedded to decompose lung images into subbands in several directions and scales. In comparison to other approaches, DT-CWT is less sensitive to noise and more efficient to detect true edges [12]. We then apply histogram thresholding in each subband to obtain high resolution areas. The

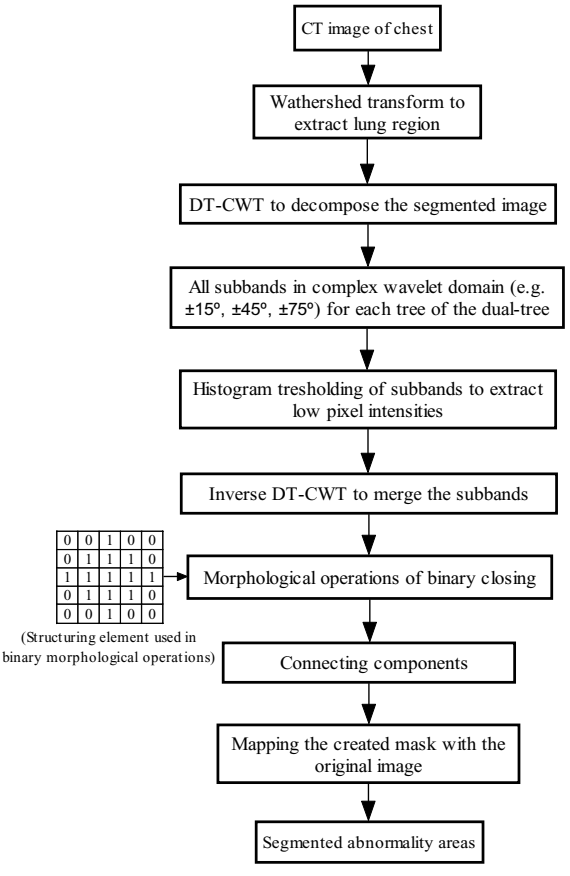

Fig. 3. Block diagram of the DT-CWT based algorithm

value of threshold is initially determined by the intensity of a specified abnormality in CT images ranging in an interval. The histogram thresholding makes this interval as narrow as possible. In case of more than one abnormality, the other abnormality intensities in CT images as well as the multilevel histogram thresholding is taken into account. After extracting the mask (Figs. 6(b), 6(e) and 6(h)) for desired intensity regions with high resolution, post-processing is applied using morphological operations in order to generate connected edges, which represents a connected detected abnormality. Morphological operations of binary closing [6] are used with the structuring element shown in Fig. 3. The structuring element is a binary 5×5 matrix whose size can be changed with respect to the image size. The connected components with a pixel count less than or greater than κ (a threshold) are assumed as noise. These components are not accepted as abnormality seeds in the respective mask. The value of κ is determined with respect to the image size and the usual size of abnormalities. It is also noted that, similar to the previous methods, value of κ should not be

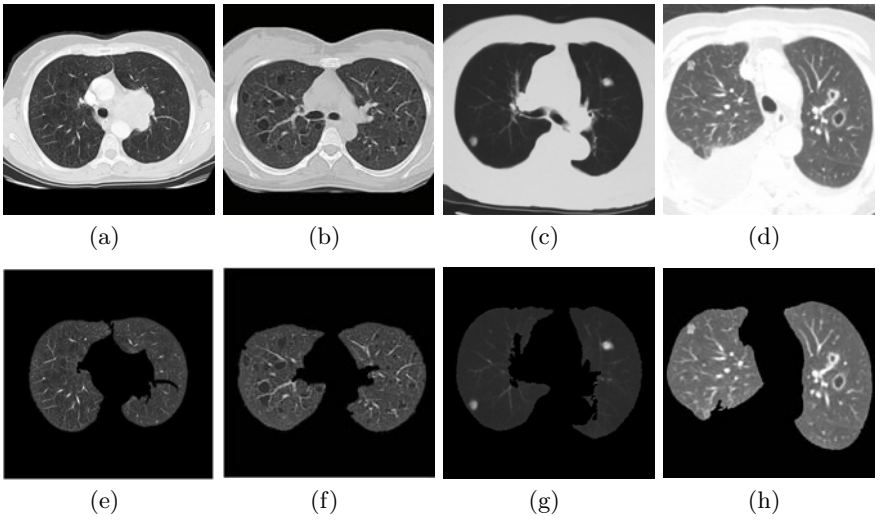

Fig. 4. Lung segmentation. (a) normal lung; (b) lung with honeycombs; (c) tumorous lung; (d) lung with cavity (right lob) and cancer (left lob); (e), (f), (g) and (h) are the segmentations for (a), (b), (c) and (d), respectively.

selected dramatically large or small. Figs. 5(a), 5(b) and 5(c) illustrate the 12 subbands (note that only wavelets are presented in this figure excluding the four scaling subbands) in the last scale of a DT-CWT decomposition for Figs. 4(f), 4(g), and 4(h), respectively. As mentioned earlier, vessel branches may also be extracted along with the thresholding procedure which are shown in Figs. 6(a), 6(d), and 6(g), if any. Finally, region detecting mask (Figs. 6(b), 6(e), 6(h)) and the segmented abnormality regions (Figs. 6(c), 6(f), 6(i)) are presented in Fig. 6.

3.2 Results and Discussion

The proposed DT-CWT based technique is applied to 75 healthy and abnormal chest images of size 512×512. The images are provided by the US National Institute of Health, NCIA section, by GE Medical Systems CT Scanners. Our early research show that the same approach using multi-wavelets gives promising results than discrete wavelets. Abnormality points (pixels) for GHM [5], GHM_{p3} and Alpert [10] multi-wavelets with repeated row pre-processing (MW_{rr}) and approximation order preserving pre-processing (MW_{ap}) are determined for reference as well. Fig. 7 shows the performance of six MW-based implementations along with the result obtained by the 9/7–10/8 DT-CWT. Scalar wavelet-based method, presented in [13], is also implemented and tested on the same sample images and shown in Fig. 7. The presented DT-CWT based approach provides better results than multi-wavelets and wavelets in general. Furthermore, MW_{rr} outperforms MW_{ap} on the average which confirms the usefulness of repeated row

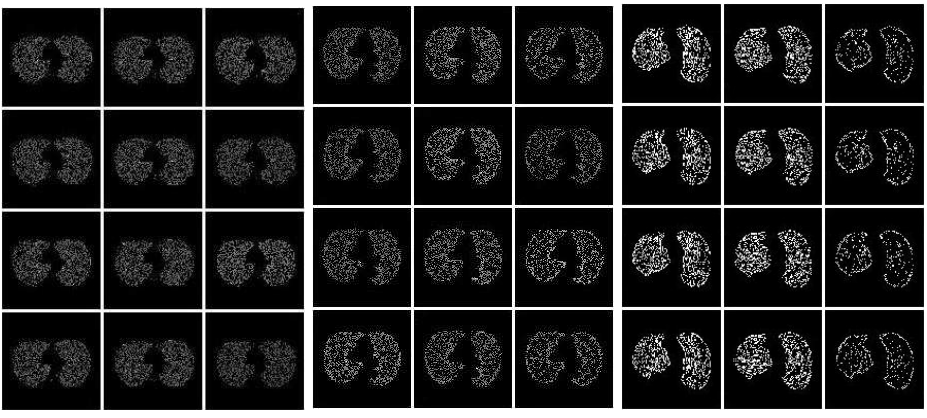

(a) (b) (c)

Fig. 5. Subbands obtained with DT-CWT in several directions. (a) lung with honeycombs; (b) tumorous lung; (c) lung with cavity and cancer.

Table 2. Statistics of different methods applied on the sample images

	DWT	Multi-wavelets	DT-CWT
Sensitivity (%)	98.6	99.9	99.9
Specificity (%)	90.3	98.1	98.5

pre-processing in detecting edges [15]. As is shown in Fig. 7, the results of the 9/7–10/8 filter bank is slightly better than the results of MW_{rr} and MW_{ap}, and significantly outperforms the results obtained by scalar wavelets [13] and previous results in [4] [16]. It is also expected to achieve significantly better results than MW_{rr}, if the amount of the design error (γ) in [17] be improved. It can be performed by the recent important work of Dumitrescu [3] proposing an SDP approximation of DT-CWT design with high accuracy, taking into account the biorthogonality and regularity constraints. As can be observed from Figs. 6(c), 6(f), 6(i) and Fig. 7, the results of the proposed DT-CWT based algorithm using the 9/7–10/8 filter bank, produce promising results for abnormality detection and segmentation in lung images than previously published results in [4] [13] [16]. The accuracy of the techniques may be shown by true positive fraction (TPF) and true negative fraction (TNF), the so-called sensitivity and specificity, which are the probability of diagnosing the presence/absence of disease when it really exists/doen not exist, respectively. Table 2 gives the statistical information obtained using the DWT, MW_{ap}, MW_{rr}, and DT-CWT. Although the statistics confirm the experimental results, this method of comparison which is also used in [13] is not reliable due to the poor outcomes of this demonstration. For instance in [13], the sensitivity of 82.5 and specificity of 99.9 in [16], has been reported to be weak compared with the sensitivity of 100 and specificity of 87.5 in [13]. Therefore, we have also investigated number of detected pixels

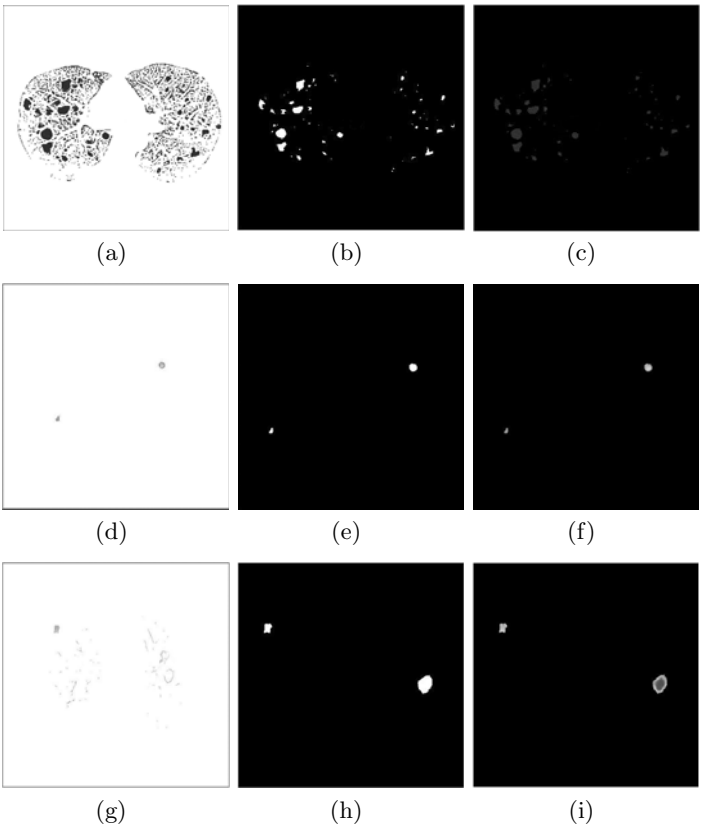

Fig. 6. Abnormalities segmentation. (a) vessel branches and honeycombs; (b) honeycombs mask; (c) segmented honeycombs; (d) no vessel branches but tumors; (e) nodules mask; (f) segmented nodules; (g) vessel branches, cavity and cancer; (h) abnormalities mask; (i) segmented abnormalities.

associated with abnormality detection in each approach for all 75 test images (14 images randomly selected to be shown here). Fig. 7 shows the performance of six MW-based implementations along with the results obtained by the 9/7–10/8 complex filter bank. In this figure, vertical axis is out of 512×512 pixels. The results obtained by DWT-based approach is also shown for reference. The proposed method in [13] gives better performance than previous studies in literature. The initial results using multi-wavelets provides better results when compared with the scalar wavelets given in general as is shown in Fig. 7. The proposed 9/7–10/8 filter bank simply outperforms the results obtained by discrete wavelets significantly and it also performs slightly better than that of the MW_{ap} and MW_{rr}.

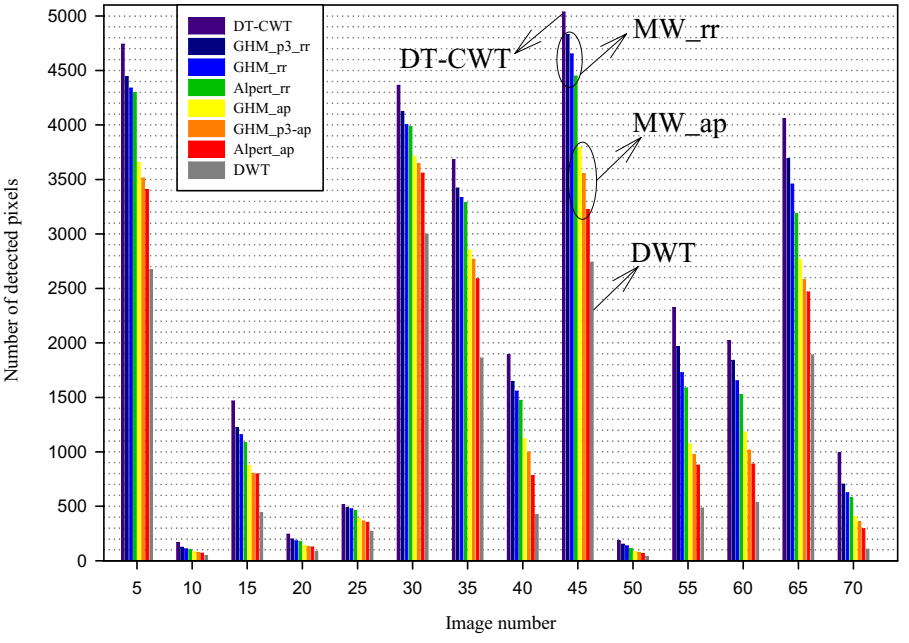

Fig. 7. Number of pixels of abnormalities in each sample image obtained by different methods

4 Conclusion

An automatic DT-CWT based method for detection and segmentation of lung abnormalities in CT images is proposed. Employing the recently designed 9/7–10/8 dual-tree complex filter bank, we take the advantage of DT-CWT in accurate boundary observation, and at the same time we apply multilevel histogram thresholding to separate different abnormalities with different resolutions. The method is very efficient in terms of its accuracy and the number of detected abnormal points. Simulation results show that the performance improvement of DT-CWT based technique is on the average over the multi-wavelets. Furthermore, the results indicate that DT-CWT outperforms both multi-wavelets and DWT in general. The boundary of segmented targets are accurately extracted in contrast with the weakness of DWT and previous techniques in that regard. This is due to good directionality and shift-invariance of dual-tree complex wavelet transform, full symmetry of our designed 9/7–10/8 filter bank, and number of vanishing moments of the 9/7–10/8 pair (4 and 3 vanishing moments for 9/7 and 10/8, respectively). In view of the success of the presented approach, and performance of 3D dual-tree complex wavelet transform in video processing [11], it is reasonable to hope promising results for 3D extraction of abnormalities in CT, PET, SPECT and MRI images.

Aknowledgement. This work is supported in part by the Canada Research Chair program and the NSERC Discovery Grant. The authors would like to

thank the US National Institute of Health for high quality database of CT images provided for research.

References

1. Baradarani, A., Wu, J.: A dual-tree complex wavelet with application in moving object segmentation. In: Proc. 19th IEEE Int. Conf. on Pattern Recog., Florida (2008)
2. Baradarani, A., Ozkaramanli, H., Ozmen, B., Demirel, H.: Multi-wavelet based moving object detection and segmentation. In: Proc. of the Global Int. Conf. on Signal Process, Santa Clara, California (2006)
3. Dumitrescu, B.: SDP approximation of a fractional delay and the design of dual-tree complex wavelet transform. IEEE Trans. on Signal Process. 56(9), 4255–4262 (2008)
4. Farag, A., El-Baz, A., Gimelfarb, G.G., Falk, R., Hushek, S.G.: Automatic detection and recognition of lung abnormalities in helical CT images using deformable templates, pp. 856–864. Springer, Heidelberg (2004)
5. Geronimo, J., Hardin, D., Massopust, P.: Fractal functions and wavelet expansions based on several scaling functions. J. Approx. Theory 78, 373–401 (1994)
6. Gonzalez, R.C., Woods, R.E.: Digital Image Process. Prentice-Hall, Englewood Cliffs (2005)
7. Huang, J.C., Su, T.S., Wang, L.-J.: Double change detection method for wavelet-based moving object segmentation. Elect. Letts. 40, 798–799 (2004)
8. Kim, C., Hwang, J.-N.: Fast and automatic video object segmentation and tracking for content based applications. IEEE Trans. on Circts. Syst. Video Technol. 12, 122–129 (2002)
9. Kingsbury, N.G.: Complex wavelets for shift invariant analysis and filtering of signals. Jour. Applied and Computational Harmonic Analysis 10(3), 234–253 (2001)
10. Ozkaramanli, H.: A unified approach for constructing multi-wavelet with approximation order using refinable super functions. IEE Proc.-Vis. Image Signal Process. 150, 143–152 (2003)
11. Selesnick, I.W., Li, K.Y.: Video denoising using 2D and 3D dual-tree complex wavelet transforms, Wavelet Applications in Signal and Image. In: Selesnick, I.W., Li, K.Y. (eds.) Proc. SPIE, San Diego, August 2003, vol. 5207 (2003)
12. Selesnick, I.W., Baraniuk, R.G., Kingsbury, N.G.: The dual-tree complex wavelet transform – a coherent framework for multiscale signal and image processing. IEEE Signal Process. Magazine 6, 123–151 (2005)
13. Shojaii, R., Alirezaie, J., Khan, G., Babyn, P.: Automatic honeycomb lung segmentation in pediatric CT images. In: IEEE Int. Symp. on Signal Process., pp. 1–4 (2007)
14. Sluimer, I., Schilham, A., Prokop, M., Ginneken, B.V.: Computer analysis of computed tomography scans of the lung: A survey. IEEE trans. on Med. Imag. 25, 385–405 (2006)
15. Strela, V., Heller, P.N., Strang, G., Topiwala, P., Heil, C.: The application of multi-wavelet filterbanks to image processing. IEEE Trans. on Image Process. 4, 548–563 (1999)
16. Uppaluri, R., Hoffman, E.A., Sonka, M., Hartley, P.G., Hunninghake, G.W., McLennan, G.: Computer recognition of regional lung disease patterns, Americ. J. Respiratory and Critic. Care Med. 160, 648–654 (1999)
17. Yu, R., Baradarani, A.: Sampled-data design of FIR dual filter banks for dual-tree complex wavelet transforms. IEEE Trans. on Signal Process. 56(7), 3369–3375 (2008)